> IEEE J. Sel. Topics Appl. Earth Obs. Remote Sens, doi:10.1109/JSTARS.2025.3631136, 2025..

Identifying and Correcting for Residual Biases in the ASCAT and ERA5 Wind Speed Products

Gopal B. Sundaram, *Student Member, IEEE*, Christopher S. Ruf, *Life Fellow, IEEE*

Abstract— **The ASCAT instrument is a real-aperture radar that operates at C-band and measures backscatter from the ocean surface, from which near surface wind speed is estimated. However, the variance of radar backscatter is not completely explained by that of the near surface wind speed, and there are other environmental factors that can also perturb the backscatter. The ASCAT wind speed retrieval algorithm attempts to correct for the other factors, and it is largely successful. We examine here two environmental factors, precipitation and atmospheric stability at the surface, which are found to correlate strongly with residual biases in the ASCAT and ERA5 wind speed products. Correction algorithms are developed to remove the dependence of bias on these two environmental variables on both wind speed products. With the corrections applied, ASCAT's mean global wind speed bias is reduced and regional variations in the bias are narrowed. As one example of the impact of the biases, they are estimated to cause a 2.1% average global error in latent heat flux transferred from the ocean to the atmosphere.**

Index Terms— **Hydrology, Precipitation, Ocean Circulation, Ocean Waves, Radar scattering, Wind speed**

I. INTRODUCTION

OCEAN winds play a critical role in Earth's climate system by driving oceanic heat transport. Heat is transported across the globe through ocean currents, which are influenced by the near surface winds. The currents transporting heat regulate temperature and influences weather patterns across the planet. Therefore, the ability to monitor and track ocean winds is critical to monitoring changes in global weather patterns. Directly measuring the wind requires devices such as an anemometer, and while these machines have been around for centuries, having an in-situ network of anemometers and monitors is impractical. Thus, we turn to satellite-borne techniques and sensors [1]. Satellite coverage allows for near real time global observations of ocean winds. These remote sensing methods are the standard observational method for the best spatial and temporal coverage.

This leads to three questions: What exactly are the satellites measuring? What kind of sensors measure wind speed? How accurate are these satellite-borne measurements? We consider answers to these questions in the following sections.

A. Wind Driven Waves

When wind blows across the surface of the water, it initiates a process that roughens the surface. The friction between the air and the water surface places stress on the surface, which transfers energy and momentum from the air to the water. The energy transfer causes the water surface to roughen, initially creating small ripples. As the wind continues to blow, the energy in these small ripples cascades into larger waves, eventually resulting in a fully developed spectrum of surface roughness [2].

The friction between the wind and the water can be intensified by unstable atmospheric conditions. Unstable atmospheric conditions occur when the sea surface temperature is warmer than the near surface air temperature, leading to warm air rising from the surface of the ocean. The sinking of higher cold air parcels and the rising of lower warm air parcels increases the vertical mixing. Vertical mixing of winds leads to an increase in turbulent flow, which leads to greater interaction between surfaces [3]. A higher rate of interaction between the atmosphere and ocean surface increases the friction between them. A common way to quantify the stability of the atmosphere is by the difference between the sea surface temperature and the near surface air temperature, henceforth referred to as the air-sea temperature difference [4].

B. Satellite Based Wind Speed Products

1) **Scatterometers**

For satellite wind products, the most common active sensor used is a scatterometer, which is a type of microwave radar [5]. Scatterometers are designed to measure the backscatter of radar signals from the Earth's surface. When a radar signal is incident on the surface of the ocean, reflection and scattering occur. The extent of the signal power that scatters in various directions is primarily determined by the roughness of the ocean surface [6]. The backscattered power received by the radar is proportional to the normalized radar cross-section, σ_0, of the surface, from which it is possible to derive the near ocean surface wind velocity [7]. Notable examples of scatterometers include

This work was supported in part by NASA through Science Mission Directorate Contract NNL13AQ00C, awarded to University of Michigan. *(Corresponding author: Gopal B. Sundaram).*

Gopal B. Sundaram is with the Department of Climate and Space Sciences and Engineering, University of Michigan, Ann Arbor, MI 48109 USA (e-mail: gopalsun@umich.edu).

Christopher S. Ruf is with the Department of Climate and Space Sciences and Engineering, University of Michigan, Ann Arbor, MI 48109 USA (e-mail: cruf@umich.edu).

Color versions of one or more of the figures in this article are available online at http://ieeexplore.ieee.org

SeaWinds [8], SCATSAT-1 [9], and ASCAT [10]. This paper focuses on the wind speeds retrieved by the ASCAT satellite system.

The Advanced Scatterometer (ASCAT) is a real aperture radar designed by the European Space Agency [11]. There have been three ASCAT instruments launched on three separate satellites. MetOP-A launched in 2006, MetOP-B in 2012, and MetOP-C in 2018. ASCAT uses C-band microwave scatterometry to determine the wind vectors over the ocean surface. ASCAT operations are crucial for weather forecasting, climate research and marine weather forecasting. ASCAT operates on a sun-synchronous polar orbit which allows it to cover the entire globe in a 3-day period [11].

2) **Relationship between Satellite Data and Wind Speed**

As mentioned above, it is possible to derive the near ocean surface wind velocity from the normalized radar cross-section (σ_0) of ASCAT. The bridge between these two variables is described by the radar range equation and geophysical modeling functions (GMFs). The radar range equation is the relationship between σ_0, and the power received by the radar, as given by

$$P_r = \frac{P_t G^2 \lambda^2 AL}{(4\pi)^3 R^4} \sigma_0 \quad (1)$$

where P_r and P_t represent the received and transmitted power, G is the antenna gain, λ is the wavelength, R is the distance from the radar to the target, A is the area of the radar target, L is a generalized loss factor that accounts for atmospheric attenuation and system loss, and σ_0 is the normalized radar cross section [12]. Everything on the right side of the equation aside from σ_0 is known from the engineering of the sensor, antenna, and spacecraft. Received power is our incoming data, so (1) can be rearranged to solve for σ_0.

The relationship between σ_0 and wind speed is determined using a geophysical modeling function (GMF). A geophysical modeling function is an empirical fit which uses a training data set to establish an empirical monotonic relationship between NRCS and wind speed. For the ASCAT operational wind product, a GMF named CMOD5 is used [13]. Since the GMF uses a global distribution of training data, it may not fully account for regional differences where conditions are significantly different from the global norm.

C. Environmental Parameters

Near ocean-surface wind velocity is not the only environmental variable that affects scatterometer retrievals. Overall, σ_0 is determined by ocean surface roughness and surface dielectric properties. Wind-driven waves affect the surface roughness through processes described below (see the Wind Driven Waves section). However, there are other environmental parameters that affect the surface dielectric properties like sea surface salinity and temperature. There are also variables that affect the received power (P_r), such as humidity and precipitation [14]. These external variables can change the received power, which can change the estimate of σ_0 and cause errors if the environmental factors are not properly corrected.

Precipitation Rate (PR) is defined as the rate at which water falls onto the surface, for a given period. Precipitation has been shown to affect remote sensing measurements of the ocean surface. It can cause attenuation of the radar signal affecting the received power in (1), increase the roughness of the ocean surface with ring-waves [15], and cause reflections off the raindrops themselves. There are a multitude of missions designed to track precipitation, one of which is the Global Precipitation Measurement (GPM) Mission. GPM has been tracking precipitation data for over ten years and is a global standard for precipitation data.

Air Sea Temperature Difference (ASTD) refers to the difference in temperature between the air just above the surface of the ocean (T_a) and the surface water itself (T_s) and is defined as

$$ASTD = T_s - T_a. \quad (2)$$

ASTD directly affects the atmospheric stability of the air-ocean boundary layer. If it is positive, the conditions are unstable. As mentioned in the Wind Driven Waves section, unstable conditions at the ocean surface lead to an increase in turbulence and vertical mixing, which enhances the surface stress on the ocean. Increasing the vertical mixing at the ocean boundary layer raises surface waves [16], which affects the relationship between ocean surface roughness and near surface wind velocity.

D. ERA5 Data & Buoy Data

The ECMWF ERA5 wind speed data product is often utilized for validation purposes due to its gap-free data and consistent spatial and temporal resolution. The ERA5 wind speed data product is produced by reprocessing current climate observations through modern data assimilation systems, integrating records from surface weather stations, satellite data, and airborne sources to create a spatially gridded dataset updated every hour [17]. This makes ERA5 useful for ASCAT data comparisons. The ERA5 from 0900 and 1000 is used to temporally interpolate an 0930 measurement. The same process is used between 2100 and 2200. This project uses this temporally interpolated ERA5 data collocated to the ASCAT orbit, at 0930 and 2130. This is true for any standard or derived ERA5 product used.

It is important to note that ERA5 is not ground truth, it is a reanalysis model [18]. Its accuracy can be affected in areas with sparse or inaccurate observations. Therefore, while ERA5 provides one means for assessing ASCAT accuracy, it is prudent to supplement it where possible with other estimates of environmental parameters. One such data source is in-situ measurements collected by ocean buoys.

Buoy measurements generally include wind speed, wind direction, sea surface temperature and 2-meter air temperature. Buoy data are accessed via the NOAA National Data Buoy Center (NDBC) [19].

E. Objectives

This paper seeks to identify and correct residual biases in the ASCAT and ERA5 wind speed products, recognizing the potential issues in both. Refining both products, even with corrections on the order of 0.5 m/s, can have a large impact on

other variables and products that use wind speed as an input. We correlate residual biases in the ERA5 and ASCAT wind speed product with two environmental variables, precipitation rate (PR) and air-sea temperature difference (ASTD). Precipitation rate (PR) and air-sea temperature difference data are taken from ERA5 reanalysis data products. After correlating the biases, a correction algorithm is developed to correct for these residual biases.

II. METHODOLOGY

A. Data Source Description

Table 1 details the specific datasets used, and includes details such as spatial and temporal gridding, version number/access date, and the URL where the datasets are available.

TABLE I
DATA DESCRIPTION AND SOURCE LOCATION

Product↓/ Descriptor →	Data type	Version Number/Access Date	Spatial/Temporal Gridding	Data Duration	URL for dataset
ERA5 2-meter air temperature (T_a)	Reanalysis Data	V5, Accessed 09/09/2024 from Copernicus Climate Data Store	0.2˚x0.2˚, 1 hour	01/01/2021-12/31/2021	https://cds.climate.copernicus.eu/datasets/reanalysis-era5-single-levels?tab=download
ERA5 Sea Surface Temperature (T_s)	Reanalysis Data	V5, Accessed 09/09/2024 from Copernicus Climate Data Store	0.2˚x0.2˚, 1 hour	01/01/2021-12/31/2021	https://cds.climate.copernicus.eu/datasets/reanalysis-era5-single-levels?tab=download
ERA5 10m Wind (U_{10})	Reanalysis Data	V5, Accessed 02/01/2024 from Copernicus Climate Data Store	0.2˚x0.2˚, 1 hour	01/01/2021-12/31/2021	https://cds.climate.copernicus.eu/datasets/reanalysis-era5-single-levels?tab=download
ERA5 10m Zero Current Equivalent Wind (U_{zc})	Modified Reanalysis Data	V1, Created 08/19/2023	0.5˚x0.5˚, 1 hour	01/01/2021-12/31/2021	Local Host
ASCAT Wind Speed (U_{ASCAT})	Satellite Data (ASCAT-C sensor, aboard MetOP-C)	V02.1, Accessed 02/01/2024 from Remote Sensing Systems	0.25˚x0.25˚, 1 day	01/01/2021-12/31/2021	ftp://ftp.remss.com/ascat
NDBC Buoy Winds (U_{BUOY})	In-situ wind speed data collected from various buoys	Accessed 03/14/2025 from NDBC	0.001˚x0.001˚, 1 hour	08/01/2018-05/31/2020	https://www.ndbc.noaa.gov/obs.shtml

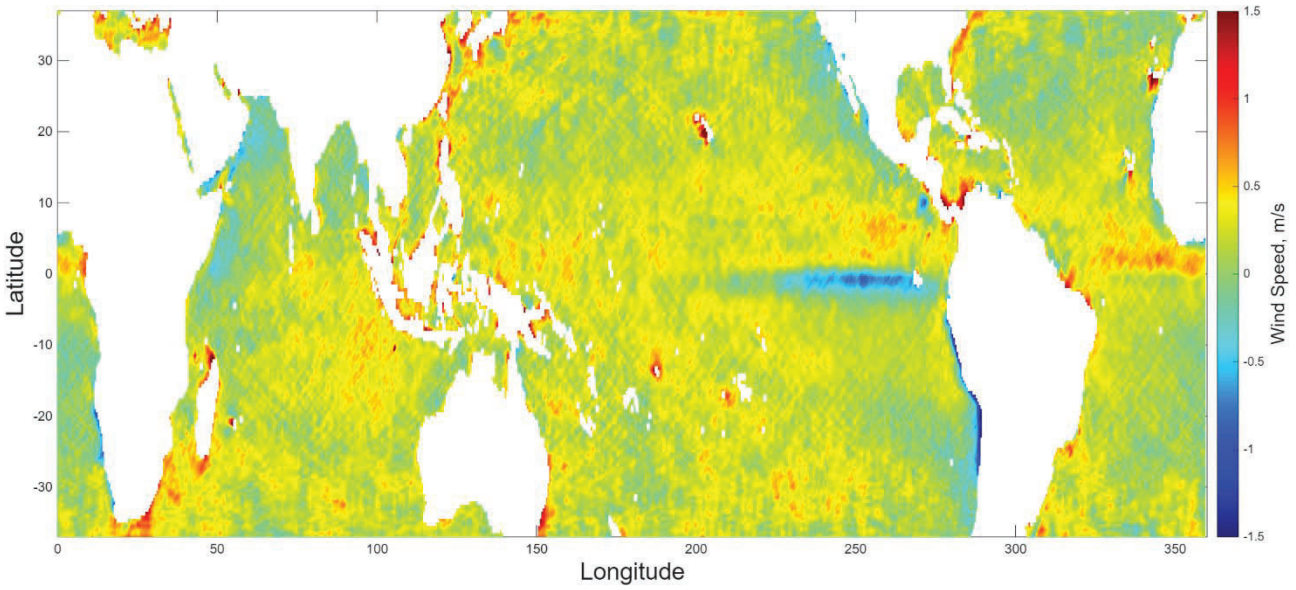


Fig. 1. ASCAT wind speed bias plot averaged over 2021. The ERA5 Zero Current Equivalent Wind is the reference wind used as ground truth. Notable areas of wind speed bias include the ITCZ, around the Kuroshio and Gulf Currents and around Indonesia.

B Exploring the Data Sources and Examining the Variables

1) Standard ASCAT Wind Speed Bias Maps

ASCAT wind speed bias is defined here as the difference between the ASCAT wind speed (U_{ASCAT}) and the ERA5 Zero Current equivalent wind speed (U_{zc}), given by

$$WSB_{ASCAT} = U_{ASCAT} - U_{ZC}. \quad (3)$$

WSB_{ASCAT} is gridded on a 0.5˚x0.5˚ grid, as U_{zc} was developed on that grid size. WSB_{ASCAT} is a daily product, which can then be averaged over seasons or the year. U_{zc} is a reference wind that takes the standard ERA5 10m winds and adjusts them for ocean surface currents. The Zero Current Equivalent Wind is used to account for the difference in reference frames between satellite-based wind products and the ERA5 reanalysis winds. See the Appendix for a full explanation of U_{zc} and its use.

To evaluate (3), the spatial and temporal grids of both righthand variables must be the same size. The temporal grid and duration are the same size, but there is a difference in the spatial grid (see Table 1). Thus, spatial regridding must be done to match the products. A nearest neighbor averaging scheme is used to change the ASCAT wind speeds from a 0.25˚x0.25˚ grid to a 0.5˚x0.5˚ grid. Fig. 1 is a global map of the wind speed bias averaged over CY 2021. Averaging over a full year shows the areas of persistent bias throughout the year, although it may wash out seasonal biases that change sign throughout the year.

As shown by Fig. 1, there are regions where persistent wind speed biases are present. The ITCZ in both the Pacific and Atlantic Oceans has a consistent positive bias, meaning ASCAT is overestimating wind speeds when compared to the model. The Gulf Stream [280˚-290˚ E, 15˚-35˚ N], the Kuroshio Current [120˚-145˚E, 15˚-35˚ N] and the Agulhas Current [25˚-35˚ E, 30˚-37˚ S] all have persistent positive wind speed biases as well. There are very few areas of negative wind speed bias, but the notable areas are around the Equatorial Counter Current directly west of the Galapagos Islands and the Western Indian Ocean. As was noted in the Introduction, environmental parameters can affect ASCAT's ability to retrieve wind speeds. In the next section, we consider possible environmental sources of the biases.

2) **Examining the Environmental Variables**

Because T_s and T_a in (2) are on the same spatial and temporal grid, they can be used directly to create a product for air-sea temperature difference. Both precipitation rate and air-sea temperature are on a finer grid resolution than the ASCAT wind speed bias, therefore a nearest neighbor algorithm is used to interpolate the environmental products. To make sense of the precipitation rate and air-sea temperature difference products, we generate histograms and cumulative distribution functions (CDFs) for each of the variables. The air-sea temperature difference histogram is binned every 0.0625˚ C, and the precipitation rate histogram is binned every 0.007 mm/hr. The histograms and CDFs are calculated after refitting the environmental data to the same resolution as the ASCAT wind speed bias data.

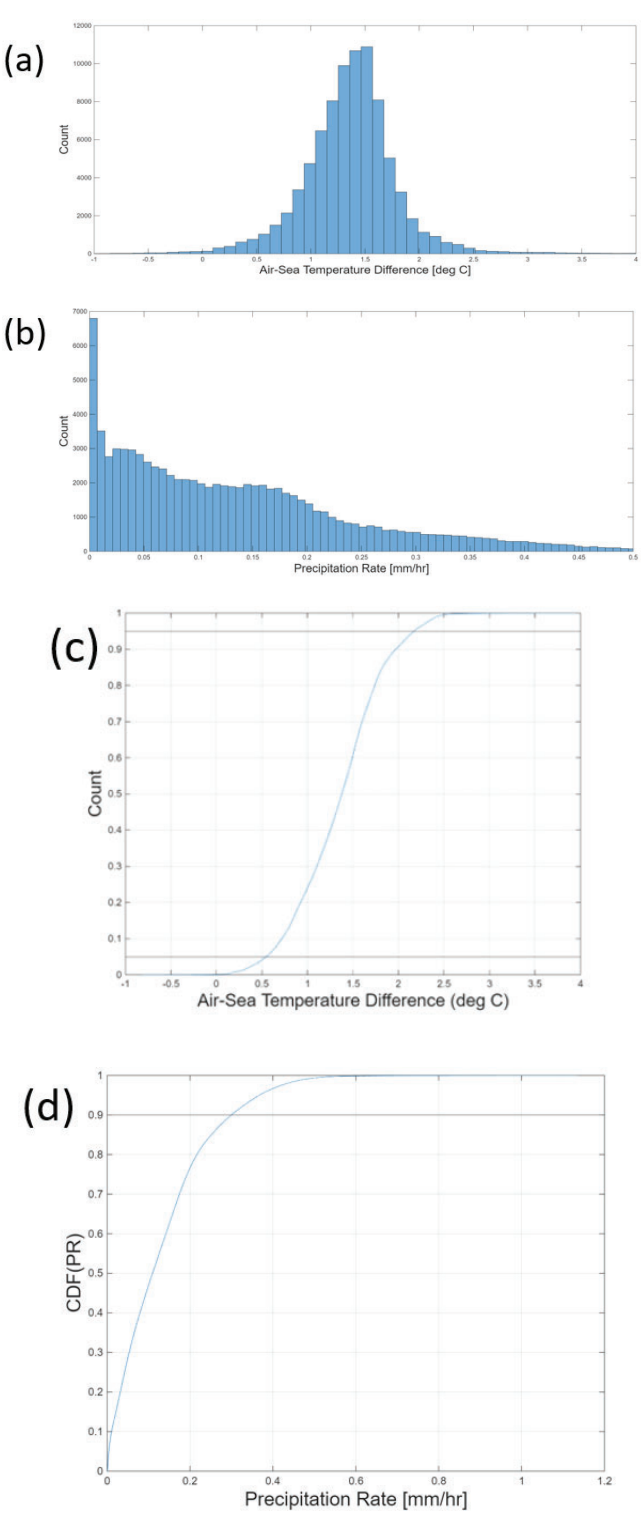


Fig. 2. (a) A histogram of air-sea temperature difference (ASTD). ASTD is gridded in 0.5x0.5˚ bins and averaged over 2021. (b) A histogram of Precipitation Rate (PR) in mm/hr. Precipitation Rate is taken from IMERG data, gridded in 0.5x0.5˚ bins and averaged over 2021. (c) A cumulative distribution function for the air-sea temperature difference. (d) A cumulative distribution function for the precipitation rate.

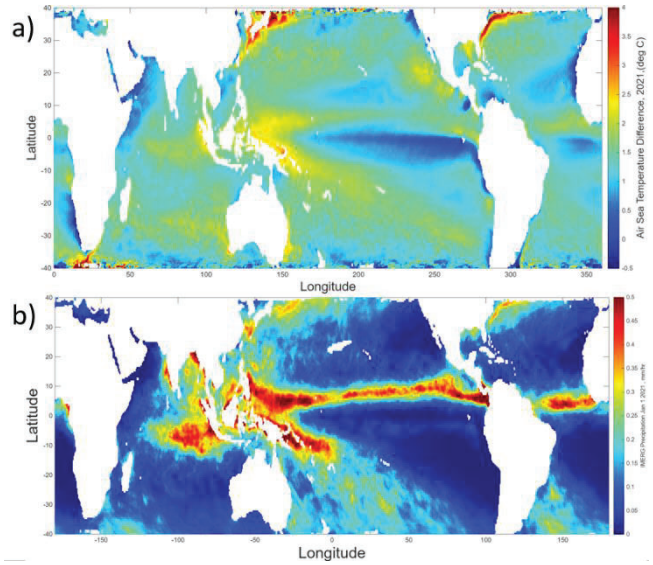


Fig. 3. (a) Map of Air Sea Temperature Difference averaged over 2021 using ERA5's 2-meter temperature and sea surface temperature. (b) Map of Precipitation Rate averaged over 2021. Precipitation Rate is taken from IMERG data.

Fig. 2(a) and 2(b) are histograms describing the distributions of the air-sea temperature difference and precipitation rate for CY 2021. The values used in the histograms collocate directly to ASCAT values at the same time. ASTD has a mean value of 1.36˚ C, and a standard deviation of 0.47˚ C. PR is a one-sided distribution, with the mode between 0-0.01 mm/hr. Fig. 2(c) and 2(d) are the cumulative distribution functions (CDFs) of the air-sea temperature difference and precipitation rate yearly gridded data. The rise on the left of Fig. 2d is due to the large amount of area that has minimal precipitation throughout the year.

Fig 2(c) and 2(d) also give us a definition for what "anomalous" means for both precipitation and air-sea temperature difference. We take the values below the 5th percentile and above the 95th percentile to define anomalously low and high air-sea temperature difference. These boundaries are 0.6˚ C and 2.02˚ C. Anomalously high precipitation is defined as a rate above the 90th percentile, which is above 0.3 mm/hr. This definition makes it easier to pinpoint anomalous regions when making maps of the environmental data products. Fig. 3a is a map of the air-sea temperature difference, gridded on a 0.5x 0.5˚grid and averaged over CY 2021. Fig. 3b is a map of the precipitation rate, gridded on a 0.5x0.5˚grid and averaged over CY 2021.

Maps of precipitation rate and air-sea temperature difference display similar characteristics to the ASCAT wind speed bias maps. Fig. 3a pinpoints many regions of anomalously high and low air-sea temperature difference. As defined earlier, anomalous regions of air-sea temperature difference are regions outside of the 0.6-2.02˚C range. The Gulf Stream, the Kuroshio Current and the Agulhas Current have anomalously high air-sea temperature differences. The water around Indonesia also has a high air-sea temperature difference. There are fewer areas of anomalously low air-sea temperature difference, but the notable

areas are around the Equatorial Counter Current directly west of the Galapagos Islands and the Western Indian Ocean.

One major feature of Fig. 3b is the large band of precipitation that extends across the ITCZ. At its peak, the rain band averages 0.6 mm/hr of rain throughout the year, which equates to 5.26 m of rain per year. The high precipitation rate band also extends over the mainland of Indonesia. The Gulf Stream and the Kuroshio Current have moderately high rates of precipitation. This is due to a phenomenon associated with sea surface temperatures. The currents transport warm, tropical water from the Equator towards the poles. The tropical water is transported north, and evaporates, rising into the atmosphere. The rising warm, moist air from the tropics increases the moisture content in the air, which leads to precipitation [20].

3) **Adjusting the standard ERA5 Winds to account for discrepancies with buoy winds**

The Eastern Pacific portion of the Intertropical Convergence Zone (ITCZ) [90-140 W, 10N-10S] is of interest as the only area exhibiting a pronounced ASCAT negative wind speed bias. We examine the source of this bias, specifically whether it arises from ASCAT or ERA5. In this section, a comparison of ERA5 with in-situ buoy data is used. We use the TAO Buoy Array [19], with buoys stationed approximately every 2 degrees in latitude and 5 degrees in longitude. Figure 4 shows the buoy locations in the Eastern Pacific ITCZ Region.

The TAO buoy array measures wind speeds every 30 minutes. The buoy locations are listed in Table 2:

TABLE II
TAO BUOY NETWORK LOCATIONS

Latitude	Longitudes
8 S	95 W, 110 W, 125 W, 155 W, 170 W
5 S	95 W, 125 W, 140 W, 155 W, 170 W
2 S	95 W, 110 W, 125 W, 140 W, 155 W, 170 W
0 N	95 W, 110 W, 125 W, 140 W, 155 W
2 N	110 W, 125 W, 140 W, 155 W, 170 W
5 N	110 W, 125 W, 140 W, 155 W, 170 W
8 N	95 W, 110 W, 125 W, 155 W, 170 W
9 N	140 W

To assess ERA5 accuracy we examine its mean difference from collocated buoy data. The ERA5 wind speed bias is given by

$$WSB_{ERA5,BUOY} = < U_{ERA5} - U_{BUOY} > \qquad (4)$$

where the expectation operator <> refers to the mean of coincident samples over the period 08/01/2018 to 05/31/2020. If the ERA5 data performs like the buoy data, $WSB_{ERA5,\,BUOY}$ will be near zero. To effectively use the buoy data, half the buoy data (all odd numbered days) are used to train the correction, and the other half are used to test the correction. To understand the data before applying any corrections, a visualization of the data is useful. Fig. 5 is a series of benchmark density scatter plots. Fig. 5a plots buoy measured wind speed versus ERA5 wind speed. Data used in the figure is from all buoy locations, on the time interval of 08/01/2018-05/30/2020. This is the baseline for the relationship between buoy winds and ERA5. The goal here is to see how effective our corrections are in removing environmentally dependent biases between ERA5 and buoy winds. Fig. 5b plots ERA5 wind speed versus ASCAT wind speed. This serves as a baseline for the correction developed for ASCAT winds.

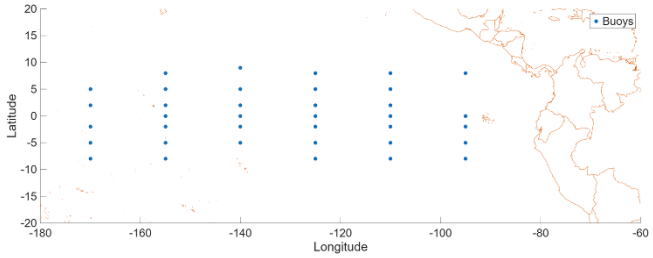


Fig. 4. Buoy locations across the Eastern Pacific. All buoys are used for the precorrection assessment. Data sampled on odd numbered days of the year are used for training the correction models, and data sampled on even days are used to evaluate the corrected ERA5 wind speed product.

As shown in Fig. 5a, buoy winds and ERA5 winds have a high correlation, with the highest density of samples closely following the 1-to-1 line of perfect agreement. Fig. 5b has markedly low correlation. This behavior is particular to the Eastern Pacific ITCZ, and this degraded behavior in ASCAT wind retrievals is a primary focus of our corrections. Both these plots will be redone with corrected data at the end of this analysis to evaluate the effectiveness of our method.

We examine the dependence of the wind speed bias on other environmental variables. If the bias depends on an environmental variable, this is an indication of a possible error in ERA5, e.g. due to improper accounting for the effects of that variable on the wind speed. Two such dependencies are considered here, those with respect to the air-sea temperature

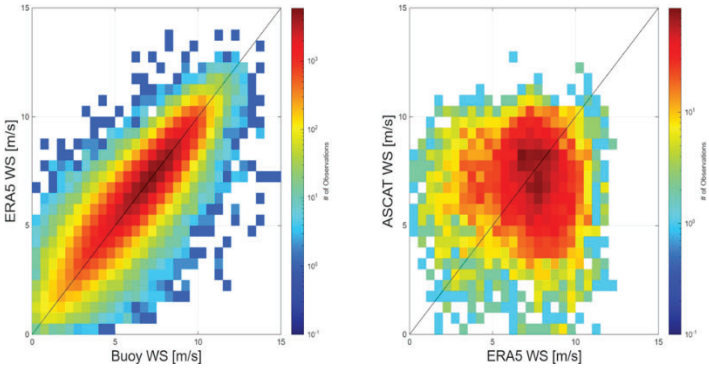


Fig. 5. (a) Density scatter plot of buoy wind speed versus standard ERA5 10m neutral wind speed (prior to any correction being applied). R^2 = 0.77 and RMSE = 0.93 m/s. (b) Density scatter plot of ERA5 wind speed versus standard ASCAT wind speed (prior to any correction being applied). R^2 = 3.5e-6 and RMSE = 2.94.

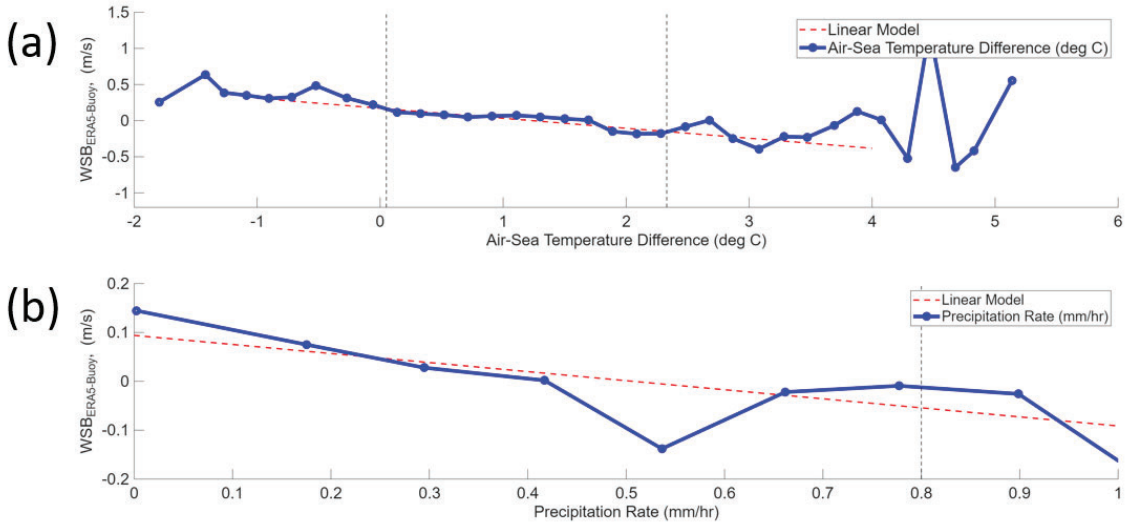


Fig. 6. (a) Buoy air-sea temperature difference plotted against $WSB_{ERA5,\,BUOY}$ (U_{ERA5}-U_{BUOY}) with a linear model fit to the data. Vertical dashed lines at 0.03˚C and 2.33˚C denote the lower and upper bounds of the 95% confidence interval. (b) IMERG precipitation rate plotted against $WSB_{ERA5,\,BUOY}$ with a linear model fit to the data. The vertical dashed line at 0.8 mm/hr represents the 97.5 percentile threshold.

difference (ASTD) and the presence of precipitation. Figure 6a plots $WSB_{ERA5,\,BUOY}$ against buoy-measured air-sea temperature difference. Figure 6b plots $WSB_{ERA5,\,BUOY}$ against the IMERG-determined precipitation rate.

Fig. 6 demonstrates a dependance of the ERA5 wind speed bias on both environmental variables. Corrections are derived to the ERA5 wind speed to remove the dependence of its bias on these two environmental variables. This correction is performed in two steps. First, we fit a least-squares polynomial curve to the dependencies shown in Fig. 6. Then an ERA5 wind speed bias correction is applied based on the polynomial curve.

In Fig. 6a, 95% of the data falls between an ASTD of 0.05˚ and 2.33˚ C. The dependence of wind speed bias on ASTD over this range is nearly linear; therefore, we use a linear fit to model the wind speed bias dependence. In Fig. 6b the data above 0.8 mm/hr accounts for only 2.5% of the data, so adjustments for the data are weighted to favor the data from 0 to 0.8 mm/hr. The dependence of wind speed bias on precipitation rate is nearly linear, therefore we use another linear fit to model the wind speed bias dependence.

The linear fit in Fig. 6a is given by

$$WSB_{ERA5,BUOY}(ASTD) = -0.138 * (ASTD) + 0.171 \quad (5)$$

where ASTD represents the air-sea temperature difference data and $WSB_{ERA5,\,BUOY}$ represents the wind speed bias between ERA5 and buoy winds. The fit in Fig 6b is given by

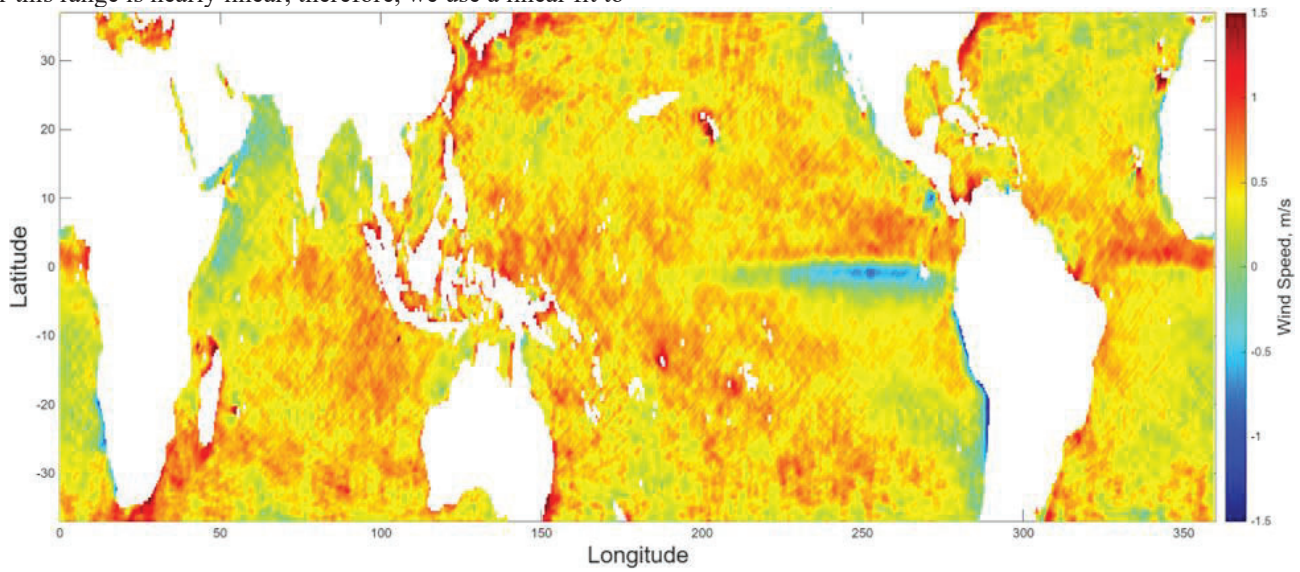


Fig. 7. ASCAT wind speed bias relative to ERA5 Environmentally Corrected wind speeds (U_{EC}). Data used in figure averaged from 01/01/2021 to 12/31/2021.

$$WSB_{ERA5,BUOY}(PR) = -0.185 * (PR) + 0.93876 \quad (6)$$

where PR represents the precipitation rate.

These adjustments are applied to the ERA5 dataset

$$U_{EC} = U_{ERA5} - WSB_{ERA5,BUOY}(ASTD) - WSB_{ERA5,BUOY}(PR). \quad (7)$$

Implementing both adjustments results in a new version of the ERA5 wind data, defined as the environmentally corrected ERA5 wind, or U_{EC}. U_{EC} will serve as the reference wind dataset for the subsequent comparison with ASCAT wind speeds. U_{EC} averaged from 01/01/2021 to 12/31/2021 is displayed in Fig. 7.

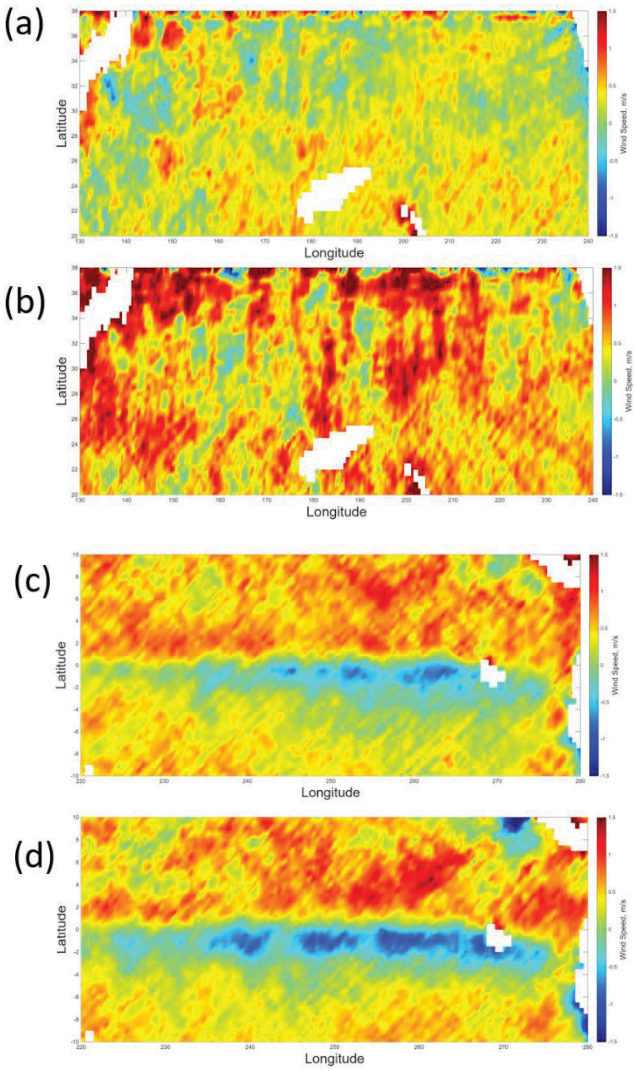


Fig. 8. Regional matchups between the Northern Hemisphere Summer (JJA) and Winter (DJF). (a) and (b) are a comparison of the North Pacific, which is overestimated in the winter months, but slightly underestimated during the summer months. (c) and (d) look at the Eastern Pacific near the Galapagos Islands, and there is a consistent underestimation of wind speed all throughout the year.

Comparing Fig. 7 to Fig. 1, there is a general increase in wind speed bias across the globe. However, wind speed bias in the Eastern Pacific ITCZ and Atlantic ITCZ have stayed largely the same. The increase in wind speed bias is not an indication of the correction failing, but rather an indication that ERA5 and ASCAT may be in more disagreement than previously perceived.

4) **Seasonal Bias Issues**

Using a yearly average instead of a seasonal average can obscure changes in the environment that happen on a seasonal scale. For section B.2 of the methodology a yearly average has been used to assess the air-sea temperature difference and the precipitation rate. While this makes it possible to see persistent regional issues across the globe, it can negate changes that occur on a seasonal basis. Fig. 8 takes the ASCAT wind speed bias data averaged in three-month seasonal periods and zooms in on the North Pacific Gyre to show a large seasonal change and the Eastern Pacific ITCZ demonstrates a small seasonal change. The easiest time to see seasonal variations is by comparing DJF and JJA maps, so those averages are used.

Fig. 8 shows snapshots of two regions. One where the seasonal and yearly averages are similar and one where the seasonal variation is obscured. Areas further from the Equator, where seasonal variations are higher, will be most impacted by this change.

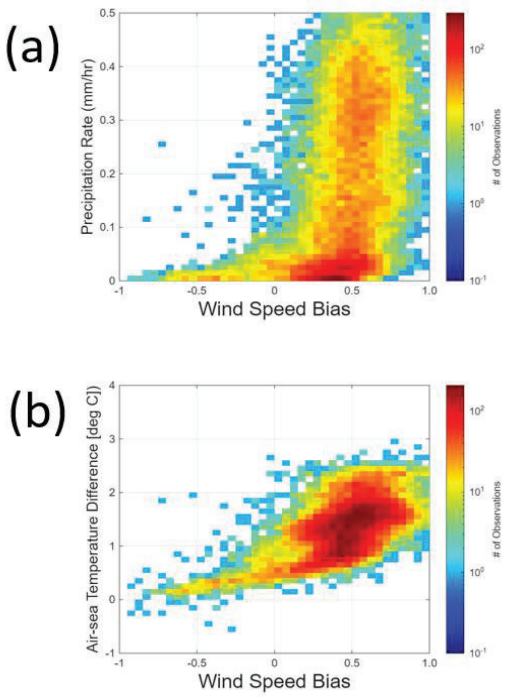


Fig. 9. (a) Density Scatter Plot of ASCAT wind speed bias and Precipitation Rate for CY2021, specifically in the ITCZ. There is a positive monotonic and linear relationship between WSB and PR. (b) Density Scatter Plot of ASCAT wind speed bias and air-sea temperature difference. There is a weak positive monotonic correlation between wind speed bias and air-sea temperature difference.

5) **Correlation between the ASCAT Wind Speed Bias and the Environmental Variables**

There are clear visual parallels between Fig. 3 and 7, particularly in the ITCZ, where there is the anomalously low region of air-sea temperature difference in the Eastern Pacific Ocean. This makes the ITCZ a good test region to check if there is a correlation between the ASCAT wind speed bias map and the environmental variables.

In Fig. 9a, there is a general positive monotonic relationship between ASCAT wind speed bias and precipitation rate. The densest region of data is around 0.5 m/s on the x axis and 0 mm/hr on the y axis, but for the points above 0.05 mm/hr, the positive monotonic relationship is clear. This means that areas of anomalously high precipitation coincide with high ASCAT wind speed bias. A similar analysis is done for ASTD in Fig. 9b, but there is a larger spread when compared with 9a. Fig. 9b also has a left-skewed tail, implying that there is a matchup between areas of anomalously low air-sea temperature difference and negative wind speed bias. Fig. 10 is a comparison of air-sea temperature difference to ASCAT wind speed bias. Both products are averaged over a year and zoom into the Eastern Pacific [220˚-280˚ E, 10˚N-10˚S] and Gulf Stream [270˚-300˚E, 15˚-37˚N] regions. These two regions are picked to display the visual alignment between the satellite product and the environmental variable.

Fig. 10 displays regions where the anomalies align. The correlations seen in the data are consistent with the physical processes that drive them, bolstering our ability to relate them as cause and effect. Precipitation Rate has a positive monotonic increase starting around 0.01 mm/hr, implying that in rainy conditions ASCAT overestimates the wind speed. Rainfall attenuates the transmitted signal, which lowers the received power [18]. Taken at face value, this suggests that wind speed should be underestimated by ASCAT. However, especially in conditions of low wind speed, rainfall can also cause an increase in backscatter

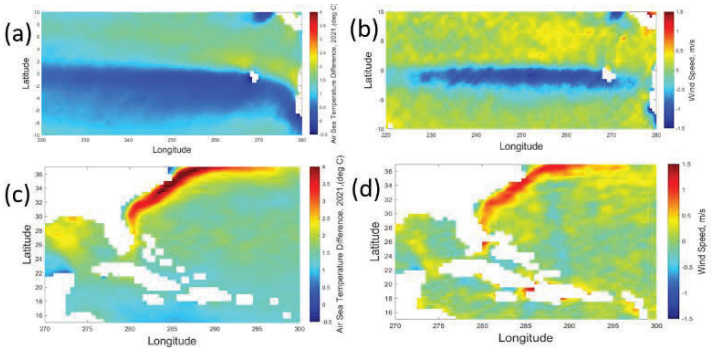


Fig. 10. Regional matchups of ASCAT wind speed bias and air-sea temperature difference. Displayed to show visual similarities between biases and environmental parameters. (a) and (b) are a comparison of the underestimated wind speed bias region of the Eastern Pacific and the anomalously low air-sea temperature difference region. (c) and (d) are a comparison of the Gulf Stream region, where anomalously high air-sea temperature difference correlates with high wind speed bias.

due to the signal scattering from raindrops back toward the sensor. In addition to this, the raindrops hitting the surface can grow centimeter-scale ring waves, roughening the surface further than normal [19].

Air-sea temperature difference in Fig. 9b has a large negative tail, which equates to ASCAT underestimating the wind speed in areas of higher atmospheric stability. Regions that are highly stable are unusual, as most of the oceans fall within ASTD = 1-2˚ C, which is mildly unstable. Having a region be this stable means there is little vertical mixing, and less vertical wind stress being placed on the ocean surface [22]. The lack of upward-directed stress leads to smaller wave generation, which is consistent with an underestimation of the wind speed [4]. The opposite is true in areas of high air-sea temperature difference, for example in the Western Boundary Currents. The increase in vertical stress at the surface generates larger waves for a given wind speed, leading to an overestimation in the wind.

C. Potential Adjustment to the Wind Speed Bias

This section attempts a first order correction to reduce or remove the biases identified in the previous sections. It is intended to illustrate the potential for such a correction. In practice, operational corrections to the retrieval algorithm would be better performed by the ASCAT Project data product developers.

The correction method is a bias subtraction, as described by the following three steps.

1) Fit a polynomial between ASCAT WSB and one of the variables. In this case, Precipitation Rate (PR) is used first. This best fit polynomial represents what the wind

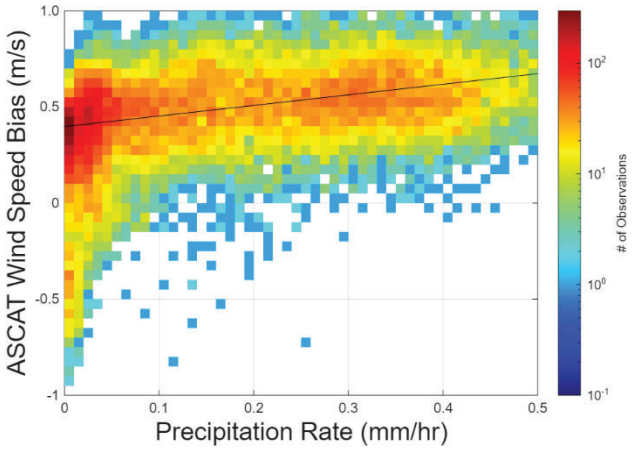


Fig. 11. Density Scatter Plot of ASCAT wind speed bias and precipitation rate, with the best fit line. Equation (8) is the wind speed bias based solely on precipitation. The axes have been flipped from Fig. 9a to keep (8) in a y = mx+b format.

speed bias would be if only based on precipitation rate, denoted as WSB(PR).

Fig. 11 adds a best fit line to Fig. 9a and rotates the axes to be in slope-intercept form. The best fit line is given by

$$WSB(PR) = 0.5504PR + 0.3978. \quad (8)$$

2) Adjust the ASCAT Wind Speeds (U_{ASCAT}) by WSB(PR) to create the Precipitation Rate Corrected ASCAT Wind Speeds ($U_{ASCAT,\,PR}$). Mathematically, this is described by

$$U_{ASCAT,PR} = U_{ASCAT} - WSB(PR). \quad (9)$$

3) Derive the new PR Corrected ASCAT wind speed bias ($WSB_{ASCAT,\,PR}$) by differencing $U_{ASCAT,\,PR}$ and the ERA5 Zero Current Equivalent Winds (U_{zc}), as given by

$$WSB_{ASCAT,PR} = U_{ASCAT,PR} - U_{zc}. \quad (10)$$

If the precipitation rate correction is done correctly, there should be no correlation between precipitation rate and the new wind speed bias. Fig. 12 is a revision of Fig. 9a using the new precipitation rate-corrected version of the ASCAT winds.

Now a similar correction can be performed for the air-sea temperature difference. The first step is to take the density scatter plot of precipitation rate corrected wind speed bias and air-sea temperature difference.

Fig. 13 differs from Fig. 9b because areas in the ITCZ have shifted in wind speed bias. This is particularly noticeable above 2˚ C. This trend is no longer linear, so a cubic polynomial is fit to the density scatter plot. Also, due to the lack of data above 2.8˚ C in the ITCZ, the training region has been updated to include the North Pacific and North Atlantic.

The data centers around 0 m/s for the wind speed bias, so this change will only affect regions of anomalous air-sea temperature

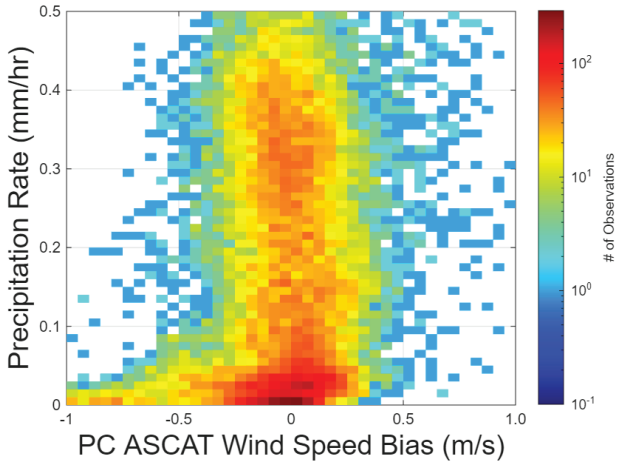


Fig. 12. Density Scatter Plot of Precipitation Rate Corrected ASCAT wind speed bias and Precipitation Rate. This figure acts as validation for the correction algorithm, as there should be no correlation between a wind speed bias that has been corrected for precipitation rate.

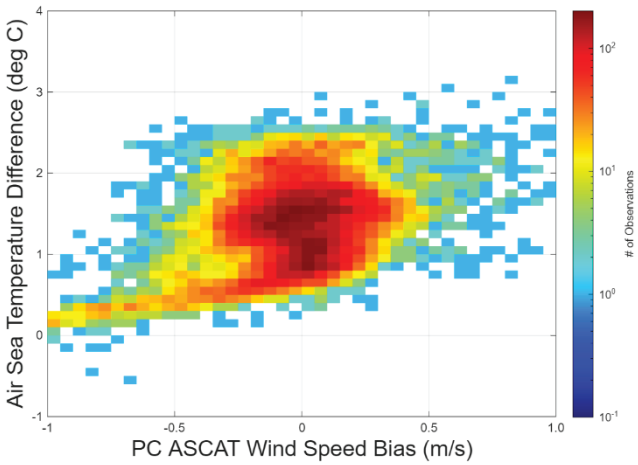


Fig. 13. Density scatter plot of Precipitation Rate Corrected ASCAT wind speed bias and air-sea temperature difference. Due to the correlation between anomalously high areas of precipitation rate and air sea temperature difference, the new matchup is slightly shifted when compared to Fig. 9b.

difference. Above 2˚ C and below 0.6˚ C a change will be made, which works well given our definitions of anomalous air-sea temperature difference. A polynomial fit could not accurately

capture both the high and low sides of the distribution, so a piecewise function was used to accurately capture the main bulk of the data and the anomalously low region. The piecewise function is given by

$$\begin{Bmatrix} WSB(ASTD) = \\ -13.961(ASTD - 0.05)^3 + 16.3224(ASTD - 0.05)^2 \\ -3.9159(ASTD - 0.05) - 0.5655 \qquad if\ 0.20 < ASTD < 0.68 \end{Bmatrix} \quad (11a)$$

$$\{WSB(ASTD) = 0.2508(ASTD) - 0.689\ if\ ASTD > 0.68\} \quad (11b)$$

$$\{WSB(ASTD) = -0.838\ if\ ASTD < 0.20\} \quad (11c)$$

where WSB(ASTD) is the wind speed bias due to air-sea temperature difference.

The piecewise fit can be explained physically by the connection between stability conditions and wind speed.

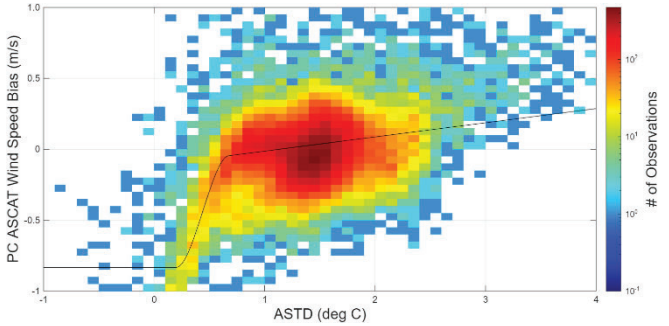


Fig. 14. Density scatter plot of Precipitation Rate Corrected ASCAT wind speed bias vs. air-sea temperature difference. The piecewise fit to the data described in (11) is shown as the black line.

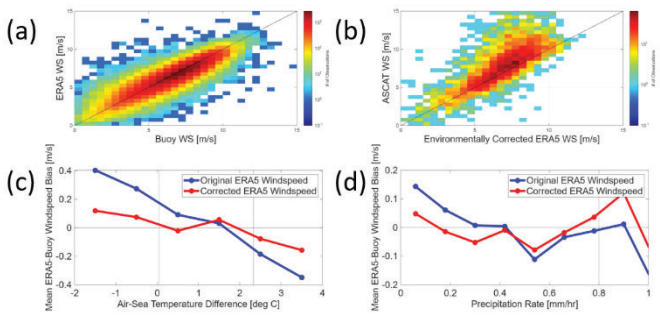


Fig. 15. (a) Density scatter plot of buoy wind speed versus environmentally corrected ERA5 wind speed. $R^2 = 0.80$ and RMSD = 0.92 m/s. (b) Density scatter plot of corrected ERA5 wind speed versus environmentally corrected ASCAT wind speed. $R^2 = 0.51$ and RMSD = 2.30 m/s. (c) $WSB_{ERA5,BUOY}$ versus Air-Sea Temperature Difference using both the original ERA5 winds and the corrected version. (d) $WSB_{ERA5,BUOY}$ versus Precipitation Rate using both the original ERA5 winds and the corrected version. The vertical dotted line signifies the 95th percentile threshold, indicating that 95% of the data is equal to or below 0.3 mm/hr.

Generally, stability conditions affect ocean wind speeds in low wind conditions, as the vertical air motions are a larger part of the overall wind stress [6]. The tail region of Fig. 14 encompasses the East Pacific ITCZ, which meets both the low wind and low stability condition. The bulk region, which exhibits average ASTD conditions stay near zero, and the high ASTD region does not have a tail effect due to it not being in a low wind regime. The monotonic section of the fit past the tail exists to stop the fit from overfitting to outliers.

Fig. 15a and Fig. 15b are the post correction assessment, formulated in the same series of benchmark plots as Fig. 5. The buoys not used for training evaluate the corrections made for both the ASCAT and ERA5 winds. There is marginal improvement in the R^2 and RMSD values for the ERA5 and buoy wind comparison, and a large improvement in the R^2 and RMSD for the ASCAT and ERA5 wind comparison. Fig. 15c and Fig. 15d use the pre and post corrected ERA5 winds to compare $WSB_{ERA5,BUOY}$ to ASTD and PR, respectively. In both cases, the curves display a reduced negative slope, suggesting the environmental variables have less influence on the ERA5 winds after correction.

The environmental correction procedure produces a new ASCAT wind speed that is bias adjusted for both PR and ASTD.

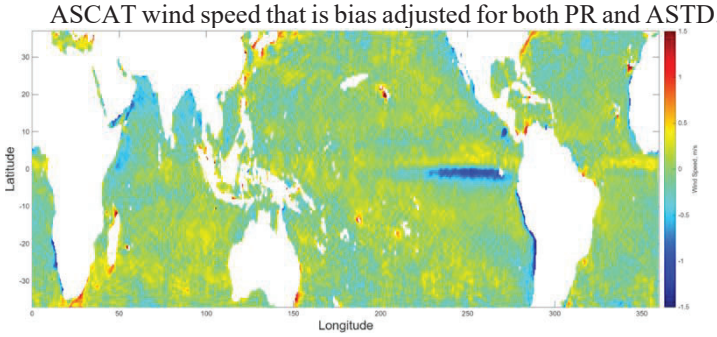


Fig. 16. ASCAT wind speed bias with a correction for Precipitation Rate. Areas of improvement include the Eastern Pacific ITCZ, Southern Pacific and around Indonesia. There are also minor improvements in the Gulf Stream and Kuroshio.

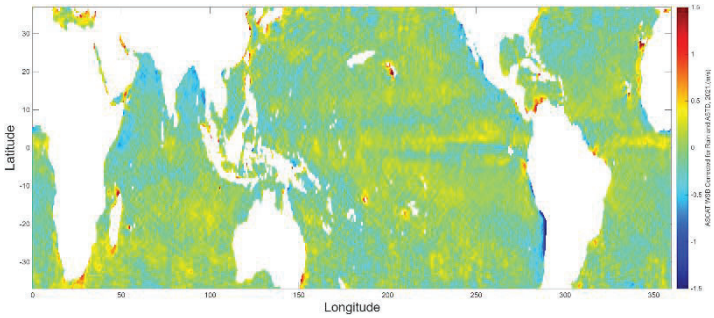


Fig. 17. The environmentally corrected wind speed bias plot, encompassing corrections for both precipitation rate and air sea temperature difference. A notable area of improvement is the Eastern Pacific ITCZ, specifically the area with a large negative air-sea temperature difference seen in Fig. 10b. This area also encompasses most of the tail region from Fig. 9b.

It is referred to as the environmentally corrected ACSAT wind speed. How the corrections affect the wind speed bias maps shown in Fig. 16 and 17 is considered in the Results section.

III. RESULTS OF BIAS CORRECTION

A. Precipitation Rate Corrected ASCAT Wind Speed Bias

Using the correction method presented in Section C of the Methodology, a plot is created of wind speed bias using the ASCAT wind speeds with a precipitation rate correction.

The precipitation rate corrected ASCAT winds significantly reduce the wind speed bias in both the Pacific and Atlantic ITCZ. The Southern Pacific, which sees a moderate amount of rain according to Fig. 3b, has also improved. The Gulf Stream and Kuroshio Current have had their biases reduced, but the improvement is minor, with the features still being visible in the plot. There is minimal change in the North Pacific, Southern Indian Ocean, and the area of large negative bias in the Eastern Pacific. This makes sense due to there being minimal precipitation present there throughout the year.

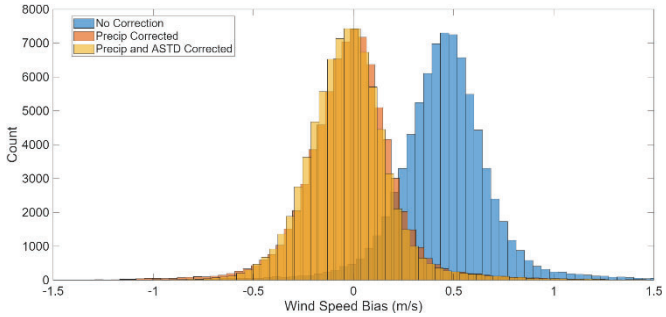


Fig. 18. A histogram of the ASCAT wind speed biases. The blue distribution is the wind speed bias using the standard ASCAT winds, the red distribution uses a precipitation rate correction, and the yellow distribution uses both precipitation rate and air-sea temperature difference corrections.

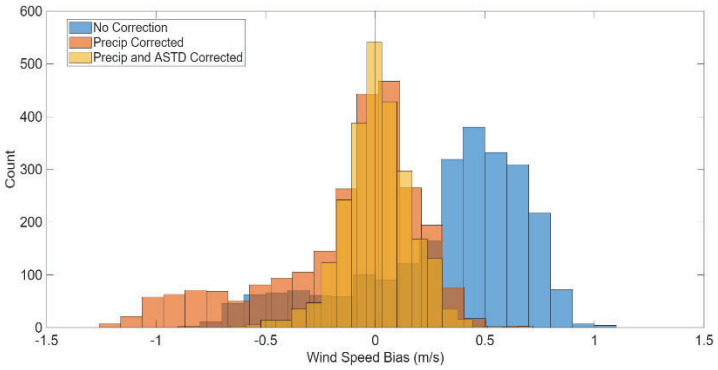


Fig. 19. A histogram of the ASCAT wind speed biases, specific to the Pacific ITCZ. The blue curve represents the standard ASCAT winds, the red curve has a precipitation rate correction, and the yellow curve is the environmentally corrected ASCAT winds.

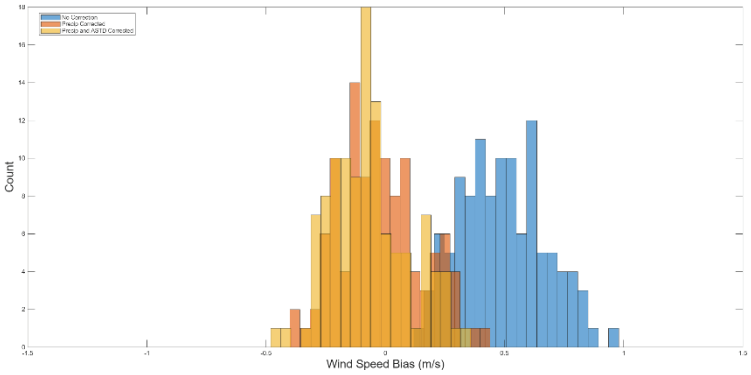


Fig. 20. A histogram of the ASCAT wind speed biases, specific to the Gulf Stream and Western North Atlantic Ocean. The blue curve represents the standard ASCAT winds, red is with a precipitation rate correction and the yellow is the environmentally corrected ASCAT winds.

B. Precipitation and Air-Sea Temperature Difference Corrected Wind Speed Bias

A similar correction can be done using air-sea temperature difference and compounded with the correction made from the precipitation rate to create the environmentally corrected ASCAT wind speed bias. The map of this is displayed in Fig. 17.

The air-sea temperature difference correction targets the anomalously low and high air-sea temperature difference areas shown in Fig. 3b. This environmentally corrected ASCAT wind speed bias is not a complete correction, as many other factors that were mentioned in Section C of the Introduction could impact the ASCAT wind speed retrieval and therefore also affect the ASCAT wind speed bias.

C. Global and Regional Analysis of the Corrections

Given these three distinct versions of ASCAT wind speed bias charts shown in Fig. 7, Fig. 16 and Fig. 17, a statistical analysis of the changes has been made. A global comparison of the mean bias and spread is shown in Fig. 18 through a histogram.

TABLE III
GLOBAL DISTRIBUTION STATISTICS

Wind speed bias Type↓/Stat→	Mean (μ)	Standard Deviation (σ)
ASCAT WSB w/no corrections	0.21 m/s	0.26 m/s
ASCAT WSB w/Precipitation Correction	-0.02 m/s	0.25 m/s
ASCAT WSB w/Precipitation and Air Sea Temperature Difference Correction	0.03 m/s	0.23 m/s

Correcting for both the air-sea temperature difference and precipitation rate reduces the mean bias from 0.21 to 0.03 m/s. The standard deviation is lowered from 0.26 to 0.23 m/s. In general, the precipitation rate correction shifts the entire distribution of errors left, and the air-sea temperature difference correction targets the tails of the distribution and narrows the spread.

Although the overall global change by the correction is positive, it is nonetheless small. Areas of anomalous environmental conditions are found to have a more significant positive correction. First, the ITCZ training region is assessed.

TABLE IV
PACIFIC ITCZ REGION HISTOGRAM STATISTICS

Wind speed bias Type↓/Stat→	Mean (μ)	Standard Deviation (σ)
ASCAT WSB w/no corrections	0.32 m/s	0.38 m/s
ASCAT WSB w/Precipitation Correction	-0.13 m/s	0.35 m/s
ASCAT WSB w/Precipitation and Air Sea Temperature Difference Correction	0.09 m/s	0.16 m/s

The Pacific ITCZ is a region of high precipitation, along with an area of anomalously low air-sea temperature difference. Adding the precipitation correction shifts the distribution left, just like the global distribution. The spread is not reduced significantly, but the air-sea temperature difference correction targets specific areas like the Eastern Pacific, so it slightly shifts the distribution while narrowing the spread.

Another region to assess is the Gulf Stream and the North

Atlantic. In the Northern Atlantic region, the addition of the air-sea temperature difference correction improved the spread, even if it shifted the mean further from zero. This is still a positive result, due to spread calculations being less susceptible to tuning issues.

TABLE V
GULF STREAM REGION HISTOGRAM STATISTICS

Wind speed bias Type↓/Stat→	Mean (μ)	Standard Deviation (σ)
ASCAT WSB w/no corrections	0.49 m/s	0.18 m/s
ASCAT WSB w/Precipitation Correction	-0.02 m/s	0.17 m/s
ASCAT WSB w/Precipitation and Air Sea Temperature Difference Correction	-0.07 m/s	0.16 m/s

IV. DISCUSSION & CONCLUSION

A. Implication for Other Products

Adjusting the ASCAT Wind Speeds has a significant impact on any geophysical parameter that uses wind speed as an input variable. Even relatively minor changes in wind speed can have significant implications on other geophysical parameters that are derived using wind speed, such as Latent Heat Flux (LHF). LHF is defined as the flux of heat from the Earth's surface to the atmosphere that is specifically associated with evaporation or condensation of water vapor at Earth's surface. It can be expressed as

$$LHF = \rho_a L_v C_E U(q_{sea} - q_{air}) \qquad (12)$$

where ρ_a is the air density over the sea, L_v is the heat of vaporization, C_E is a drag coefficient, q_{sea}-q_{air} is air-sea humidity difference and U is the near surface wind speed [23].

LHF is a vital component of Earth's energy balance budget, and significant changes in LHF can have a noticeable effect on applications such as numerical weather prediction. Even with a change in wind speed as small as 0.1 m s^{-1} over a 1-degree grid cell, the LHF can change by up to 0.35 W m^{-2}., or by $3.5x10^9$ Watts when averaged over the full grid cell.

To better appreciate the magnitude of the change, a LHF calculation using (12) has been made using the standard winds and comparing them to the environmentally corrected winds, globally and regionally. Aside from U, the variables needed for the RHS of (12) are taken from ECMWF's Copernicus Climate Data Store. The reanalysis data is regirded from its native 0.2˚x0.2˚ grid to 0.5˚x0.5˚ grid to match the standard and environmentally corrected winds. Regionally, the Gulf Stream [280˚-290˚E, 22˚-33˚N], and Pacific ITCZ [125˚-260˚E, 10˚N-10˚S] are used as test regions. The COARE algorithm was used to calculate the results [23]. Calculating LHF using the COARE algorithm gives a result per grid cell in W/m^2, so each 0.5˚x0.5˚ grid cell is multiplied by its area in square meters and summed over its respective region. The results are tabulated in Table VI.

The global LHF changes from the standard to the environmentally corrected winds amount to 3.0×10^{14} Watts, which is a 2.1% change.

This paper identifies and suggests corrections for residual biases in the ASCAT wind speed product and it offers evidence that some of the residual biases are due to environmental factors such as atmospheric stability and precipitation. While these biases are small, it is important to correct for them as even a minor change in the wind speed can have a large effect on other variables, as seen by the 2.1% change in global LHF. The correction algorithm used earlier is one method of correcting for these biases, but it is important to reiterate that operational corrections to the retrieval algorithm would be better performed by the ASCAT Project data product developers.

TABLE VI
CHANGE IN LATENT HEAT FLUX

Coverage Area↓/LHF Product→	LHF using ERA5 Uzc Winds	LHF using Standard ASCAT Winds	LHF using Environmentally Corrected ASCAT Winds	LHF Difference
Global	13.6 $x10^{15}$ Watts	14 $x10^{15}$ Watts	13.7 $x10^{15}$ Watts	3.0 x 10^{14} Watts
Gulf Stream	1.4 $x10^{15}$ Watts	1.6 $x10^{15}$ Watts	1.5 $x10^{15}$ W	1.0 $x10^{14}$ Watts
Pacific ITCZ	4 $x10^{15}$ Watts	3.8 $x10^{15}$ Watts	3.85 $x10^{15}$ Watts	5.0 $x10^{13}$ Watts

APPENDIX 1

Throughout this paper, instead of using the standard ERA5 10-meter winds, a different reference wind is used. This reference wind is the zero-current equivalent wind, denoted U_{zc}. Appendix 1 is dedicated to explaining why it is used.

The quantities being measured by satellite sensors are related to ocean surface properties that are influenced by the relative motion between the air and the water surface, rather than the motion of air parcels relative to an Earth-fixed coordinate system. However, conventional weather and climate models consider wind to be the air motion in relation to an Earth-fixed coordinate system, rather than a water surface relative coordinate system. Thus, a discrepancy exists between remotely sensed wind products and reanalysis wind

products due to the motion of the ocean surface relative to an Earth-fixed coordinate system. The main driver of the ocean surface motion is surface currents.

Ocean currents are the continuous, predictable, and directed movements of seawater. They are driven by wind, water density differences, and gravitational tides [24]. Examples of major ocean currents include the North and South Equatorial Currents, the Gulf Stream, and the Kuroshio Current. The Equatorial Currents are located around the Intertropical Convergence Zone (ITCZ) and are primarily westward moving currents. The Gulf Stream is located at the Western boundary of the North Atlantic Ocean, and Kuroshio is located at the Western boundary of the North Pacific Ocean [25].

To account for these ocean surface currents, a new reference wind speed called the zero current equivalent wind (U_{zc}) is introduced to represent the relative motion between the atmosphere and the ocean surface. This new current-adjusted wind product is intended to assess the validity of satellite wind products more accurately and to identify the root cause of some of their previously reported regional wind retrieval biases.

Generation of a zero current equivalent wind begins with selection of a model-based wind product. The ECMWF Reanalysis v5 (ERA5) Winds [26] denoted as U_{ERA5}, are used. ERA5 data is a blend of past weather data rerun with modern weather prediction models, to help fill in the gaps the weather data missed. It provides a consistent wind speed data product on an hourly basis and a 0.2˚x0.2˚grid.

The ERA5 Winds are adjusted using the Ocean Surface Current Analyses Real-time (OSCAR) Currents, denoted as U_{OSCAR}. OSCAR Currents are released every five days on a 0.33˚x0.33˚ grid [27]. The difference in grid size is because the currents do not typically change on the same spatial and temporal scales as the winds. Because of the difference in spatial gridding, a regridding of one variable to match the other is performed. Once these two variables have been spatially and temporally gridded to match, a simple vector wise subtraction is made, given by

$$U_{zc} = |\boldsymbol{U}_{ERA5} - \boldsymbol{U}_{OSCAR}| \qquad (A1)$$

Equation (A1) can be shown in component form to fully display what operations are being performed. For Eqn. 2, U is the zonal component of the data product, and V is the meridional component.

$$U_{zc} = \sqrt{(U_{ERA5} - U_{OSCAR})^2 + (V_{ERA5} - V_{OSCAR})^2} \qquad (A2)$$

This vector subtraction leads to winds that are modified by the currents. This new set of modified winds is referred to as U_{zc}.

References and Footnotes

A. References

[1] F. M. Naderi, M. H. Freilich, and D. G. Long, "Spaceborne radar measurement of wind velocity over the ocean-an overview of the NSCAT scatterometer system," *Proc. IEEE*, vol. 79, no. 6, pp. 850–866, Jun. 1991, doi: 10.1109/5.90163.

[2] N. Pizzo, L. Deike, and A. Ayet, "How does the wind generate waves?," *Physics Today,* vol. 74, no. 11, pp. 38–43, Nov. 2021, doi: 10.1063/PT.3.4880.

[3] A. A. Grachev and C. W. Fairall, "Upward Momentum Transfer in the Marine Boundary Layer," *Journal of Physical Oceanography,* vol. 31, no. 7, pp. 1698-1711, Jul. 2001, doi: 10.1175/1520-0485(2001)031<1698:UMTITM>2.0.CO;2

[4] R. G. Fleagle, "Note on the effect of air-sea temperature difference on wave generation," *Eos, Transactions American Geophysical Union,* vol. 37, no. 3, pp. 275-277, 1956, doi:10.1029/TR037i003p00275.

[5] F. J. Wentz, "Measurement of oceanic wind vector using satellite microwave radiometers," *IEEE Transactions on Geoscience and Remote Sensing*, vol. 30, no. 5, pp. 960–972, Sep. 1992, doi: 10.1109/36.175331.

[6] F. T. Ulaby and D. G. Long, "Radar Remote Sensing of the Ocean" in *Microwave Radar and Radiometric Remote Sensing,* 1st ed. Ann Arbor, MI, U.S.A: UofM Press, 2014, ch. 16, sec. 3, pp. 788

[7] R. K. Moore and W. J. Pierson, "Measuring sea state and estimating surface winds from a polar orbiting satellite", in *International Symposium on Electromagnetic Sensing of the Earth from Satellites*, Miami Beach, Fla., U.S.A, 1965;

[8] T. Lungu, "QuikSCAT science data product user's manual: Overview and geophysical data products," JPL D-18053, Version 2.2, Jet Propulsion Laboratory, Pasadena, CA, 2001, pp. 95

[9] R. Kumar et al., "Post-launch calibration-validation and data quality evaluation of SCATSAT-1," *Curr. Sci.,* vol. 117, pp. 973-982, 2019

[10] K. D. Klaes et al., "An introduction to the EUMETSAT polar system," *Bull. Amer. Meteor. Soc.,* vol. 88, pp. 1085-1096, 2007.

[11] K. D. Klaes, "The EUMETSAT Polar System," in *Comprehensive Remote Sensing,* vol 1, Oxford: Elsevier, 2018, pp. 192-219. Doi: 10.1016/B978-0-12-409548-9.10318-5.

[12] F. T. Ulaby and D. G. Long, "Radar Scattering" in *Microwave Radar and Radiometric Remote Sensing,* 1st ed. Ann Arbor, MI, U.S.A: UofM Press, 2014, ch. 5, sec. 5, pp. 170

[13] H. Hersbach, A. Stoffelen, and S. de Haan, "An improved C-band scatterometer ocean geophysical model function: CMOD5," *Journal of Geophysical Research: Oceans*, vol. 112, no. C3, 2007, doi: 10.1029/2006JC003743.

[14] N. C. Yi Lim *et al.*, "Review of Temperature and Humidity Impacts on RF Signals," in *2020 13th International UNIMAS Engineering Conference (EnCon)*, Oct. 2020, pp. 1–8. doi: 10.1109/EnCon51501.2020.9299327.

[15] L. F. Bliven, H. Branger, P. Sobieski, and J. P. Giovanangeli, "An analysis of scatterometer returns from a water surface agitated by artificial rain: evidence that ring-waves are the main feature," *International Journal of Remote Sensing*, vol. 14, no. 12, pp. 2315–2329, Aug. 1993, doi: 10.1080/01431169308954039.

[16] A. A. Grachev, C. W. Fairall, J. E. Hare, J. B. Edson, and S. D. Miller, "Wind Stress Vector over Ocean Waves," Nov. 2003, Accessed: Feb. 28, 2025. [Online]. Available: https://journals.ametsoc.org/view/journals/phoc/33/11/1520-0485_2003_033_2408_wsvoow_2.0.co_2.xml

[17] H. Hersbach et al., "ERA5 hourly data on single levels from 1940 to present," Copernicus Climate Change Service (C3S) Climate Data Store (CDS), 2023. [Online] Available: doi:10.24381/cds.adbb2d47. Accessed: Sep. 5, 2023.

[18] Belmonte Rivas, M. and Stoffelen, A.: Characterizing ERA-Interim and ERA5 surface wind biases using ASCAT, Ocean Sci., 15, 831–852, https://doi.org/10.5194/os-15-831-2019, 2019

[19] R. Crout and D. Petraitis, "Physical and meteorological data from the Tropical Atmosphere Ocean (TAO) array in the tropical Pacific Ocean. [9N-8S, 95-140W] NOAA National Data Buoy Center (NDBC), NOAA National Centers for Environmental Information, Accessed on [03/12/2025]}, Dataset. {Link: https://ncei.noaa.gov/access/metadata/landing-page/bin/iso?id=gov.noaa.nodc:NDBC-TAOBuoy}

[20] R. Seager and I. R. Simpson, "Western boundary currents and climate change," *Journal of Geophysical Research: Oceans*, vol. 121, no. 9, pp. 7212–7214, 2016, doi: 10.1002/2016JC012156.

[21] G. Delrieu, H. Andrieu, and J. D. Creutin, "Quantification of Path-Integrated Attenuation for X- and C-Band Weather Radar Systems Operating in Mediterranean Heavy Rainfall," *J. Appl. Meteor.*, vol. 39,

no. 6, pp. 840–850, Jun. 2000, doi: 10.1175/1520-0450(2000)039<0840:QOPIAF>2.0.CO;2.
[22] N. J. M. Laxague and C. J. Zappa, "The Impact of Rain on Ocean Surface Waves and Currents," *Geophysical Research Letters*, vol. 47, no. 7, p. e2020GL087287, 2020, doi: 10.1029/2020GL087287.
[23] G. R. Foltz, R. Hummels, M. Dengler, R. C. Perez, and M. Araujo, "Vertical Turbulent Cooling of the Mixed Layer in the Atlantic ITCZ and Trade Wind Regions," *Journal of Geophysical Research: Oceans*, vol. 125, no. 2, p. e2019JC015529, 2020, doi: 10.1029/2019JC015529.
[24] R. Foody, S. Dong, M. Goes, R. Campos, P. Pena, and Z. Barton, "Assessing Air–Sea Surface Turbulent Heat Fluxes from Reanalyses Using Concurrent Shipboard Measurements," Dec. 2024, doi: 10.1175/JTECH-D-24-0028.1.
[25] J. B. Edson *et al.*, "On the Exchange of Momentum over the Open Ocean," Aug. 2013, doi: 10.1175/JPO-D-12-0173.1.
[26] R. Marsh and E. van Sebille, "Chapter 4 - Western boundary currents and drifting organisms," in *Ocean Currents*, R. Marsh and E. van Sebille, Eds., Elsevier, 2021, pp. 103–143. doi: 10.1016/B978-0-12-816059-6.00014-0.
[27] K. Dohan, "Ocean Surface Current Analyses Real-time (OSCAR) Surface Currents - Interim 0.25 Degree (Version 2.0)," Ver. 2.0, PO.DAAC, CA, USA, 2022. [Online]. Available: https://doi.org/10.5067/OSCAR-25I20. Accessed: Sep. 5, 2023.



Gopal B. Sundaram (Student Member, IEEE) received the B.S. degree in physics from Case Western Reserve University, Cleveland, OH, and is pursuing the Ph.D. degree in climate and space sciences and engineering at the University of Michigan. His research interests include remote sensing methods and applications, specifically for marine litter. Mr. Sundaram is a member of the American Meteorological Society, and member of the American Geophysical Union. He serves as the Vice President of the IEEE Student Chapter at the University of Michigan.



Christopher S. Ruf received the B.A. degree in physics from Reed College, Portland, OR, and the Ph.D. degree in electrical and computer engineering from the University of Massachusetts at Amherst. He is currently the Frederick Bartman Collegiate Professor of Climate and Space Science and Director of the Space Institute, University of Michigan, Ann Arbor, MI. He has worked previously for Intel Corporation, Aloha, OR, Hughes Space and Communication, El Segundo CA, the NASA Jet Propulsion Laboratory, Pasadena, CA and Penn State University, University Park, PA. His research interests include remote sensing methods, applications, and technology. Prof. Ruf is a fellow of the American Meteorological Society, Vice Chair for Commission F of the U.S. National Committee of the International Radio Science Union, and a member of the American Geophysical Union. He is former Editor-in-Chief of the IEEE Transactions on Geoscience and Remote Sensing and has served on the Editorial Board of Radio Science, the Journal of Atmospheric and Oceanic Technology, and Scientific Reports.